Monthly Notices of the ROYAL ASTRONOMICAL SOCIETY

MNRAS **520,** 3436–3442 (2023) https://doi.org/10.1093/mnras/stad384
Advance Access publication 2023 February 06

Monitoring observations of SMC X-1's excursions (MOOSE) – II. A new excursion accompanies spin-up acceleration

Chin-Ping Hu [1]★ Kristen C. Dage,[2,3] William I. Clarkson,[4] McKinley Brumback,[5] Philip A. Charles,[6] Daryl Haggard,[2,3] Ryan C. Hickox,[7] Tatehiro Mihara,[8] Arash Bahramian [9] Rawan Karam,[2,3] Wasundara Athukoralalage,[10] Diego Altamirano,[6] Joey Neilsen[11] and Jamie Kennea[12]

[1]*Department of Physics, National Changhua University of Education, Changhua 50007, Taiwan*
[2]*Department of Physics, McGill University, 3600 University Street, Montréal, QC H3A 2T8, Canada*
[3]*Trottier Space Institute at McGill, 3550 University Street, Montréal, QC H3A 2A7, Canada*
[4]*Department of Natural Sciences, University of Michigan–Dearborn, 4901 Evergreen Road, Dearborn, MI 48128, USA*
[5]*Department of Astronomy, University of Michigan, 1085 South University Avenue, Ann Arbor, MI 48109, USA*
[6]*Physics and Astronomy, University of Southampton, Southampton, Hampshire SO17 1BJ, UK*
[7]*Department of Physics and Astronomy, Dartmouth College, 6127 Wilder Laboratory, Hanover, NH 03755, USA*
[8]*MAXI Team, Institute of Physical and Chemical Research (RIKEN), 2-1, Hirosawa, Wako, Saitama 351-0198, Japan*
[9]*International Centre for Radio Astronomy Research – Curtin University, GPO Box U1987, Perth, WA 6845, Australia*
[10]*Department of Physics and Astronomy, Michigan State University, East Lansing, MI 48824, USA*
[11]*Department of Physics, Villanova University, Villanova, PA 19085, USA*
[12]*Department of Astronomy and Astrophysics, The Pennsylvania State University, University Park, PA 16802, USA*

Accepted 2023 January 28. Received 2023 January 24; in original form 2022 December 19

ABSTRACT

SMC X-1 is a high-mass X-ray binary showing superorbital modulation with an unstable period. Previous monitoring shows three excursion events in 1996–1998, 2005–2007, and 2014–2016. The superorbital period drifts from $\gtrsim$60 to $\lesssim$40 d and then evolves back during an excursion. Here, we report a new excursion event of SMC X-1 in 2020–2021, indicating that the superorbital modulation has an unpredictable, chaotic nature. We trace the spin-period evolution and find that the spin-up rate accelerated 1 yr before the onset of this new excursion, which suggests a possible inside-out process connecting the spin-up acceleration and the superorbital excursion. This results in a deviation of the spin-period residual, similar to the behaviour of the first excursion in 1996–1998. In further analysis of the pulse profile evolution, we find that the pulsed fraction shows a long-term evolution and may be connected to the superorbital excursion. These discoveries deepen the mystery of SMC X-1 because they cannot be solely interpreted by the warped-disc model. Upcoming pointed observations and theoretical studies may improve our understanding of the detailed accretion mechanisms taking place.

Key words: accretion, accretion discs – stars: pulsars – X-rays: binaries: individual: SMC X-1.

1 INTRODUCTION

SMC X-1 is a high-mass X-ray binary consisting of an accreting neutron star and a supergiant companion (Reynolds et al. 1993; van der Meer et al. 2007). Its pulsation period is 0.7 s and the source has steadily spun up since discovery, implying a Roche lobe overflow stream-fed accretion mode (Lucke et al. 1976; İnam, Baykal & Beklen 2010; Hu et al. 2019). The orbital period of SMC X-1 is 3.89 d and decays with a rate ($\dot{P}_{\rm orb}$) of $\approx 3.8 \times 10^{-8}$ (Wojdowski et al. 1998; Falanga et al. 2015; Hu et al. 2019). A quasi-periodic superorbital modulation of this system has long been observed in the X-ray band (e.g. Gruber & Rothschild 1984; Clarkson et al. 2003a).

Radiation-driven warping is expected to be significant in stream-fed X-ray binaries with high central accretion luminosity and a physically large accretion disc (Pringle 1996; Ogilvie & Dubus 2001). The disc of such a system is unstable to warping driven by the interception and re-radiation of accretion luminosity from the compact object and inner disc. Our line of sight to the neutron star is then subject to obscuration by the warped region, leading to superorbital variation as the disc precesses. A few sources, such as Her X-1, LMC X-4, and MAXI J1820+070, are believed to have similar structures (Clarkson et al. 2003b; Thomas et al. 2022). This mechanism has been reproduced in hydrodynamical simulations of X-ray binaries (Foulkes, Haswell & Murray 2010). The stability analysis of Ogilvie & Dubus (2001) suggests that the character and precessional behaviour of a radiation-driven disc warp can be parametrized by the binary separation and mass ratio, leading to precession that could be stable, quasi-periodic, or aperiodic. A larger binary separation results in a more complicated behaviour, and SMC X-1 is in the regime of marginal instability of the warp (e.g. Charles et al. 2008).

Consistent with this prediction, the superorbital X-ray variability of SMC X-1 is known to not be strictly periodic. Variability in the time-scale of its superorbital X-ray modulation was shown early in the lifetime of the *Rossi X-ray Timing Explorer* (*RXTE*) mission

★ E-mail: cphu0821@cc.ncue.edu.tw

© 2023 The Author(s)
Published by Oxford University Press on behalf of Royal Astronomical Society

Downloaded from https://academic.oup.com/mnras/article/520/3/3436/7028790 by National Central University user on 24 February 2023

(Wojdowski et al. 1998). The superorbital modulation of SMC X-1 is punctuated by superorbital excursion events (hereafter *superorbital excursions)*, where the superorbital period shortens from $\gtrsim$60 to $\lesssim$ 40 d and then evolves back on a time-scale of 2–3 yr. Excursions have occurred at least three times in the intervals 1996–1998 (first), 2005–2007 (second), and 2014–2016 (third) (Trowbridge, Nowak & Wilms 2007; Hu et al. 2011; Dage et al. 2019; Hu et al. 2019).

SMC X-1 is a particularly valuable source because it shows variations both in superorbital modulation and in its pulse period, and thus the behaviour of the accretion engine and of its large, complicated accretion disc can be tracked together. For example, the spin-up rate increased during the first excursion, but similar behaviour was not observed in the third excursion (İnam et al. 2010; Dage et al. 2019; Hu et al. 2019).

Recent studies on pulsating ultraluminous X-ray sources (PULXs), accreting pulsars with extremely high luminosities up to ∼100 times the Eddington luminosity, suggest that a significant fraction of PULXs exhibit superorbital modulations (Bachetti et al. 2014; Kong et al. 2016; Walton et al. 2016; Hu et al. 2017; Brightman et al. 2020). Their superorbital modulations are argued to trace intrinsic changes in the mass accretion rate, and the propeller effect could be observed in these PULXs if their magnetospheric radii are similar to the co-rotation radius (Tsygankov et al. 2016; Vasilopoulos et al. 2021). Other models, such as those involving the precession of the disc or conical wind, are also suggested (Dauser, Middleton & Wilms 2017; King & Lasota 2019). Owing to its high peak luminosity (up to a few times Eddington), strong observed changes in the pulsed fraction (PF), and possible intrinsic mass accretion rate variability, SMC X-1 could be a useful local analogue to PULXs (Pike et al. 2019). Investigating the superorbital modulation of SMC X-1 in detail is therefore not only a key to understanding the accretion physics but also may hint at the nature of PULXs.

All these special properties make SMC X-1 a unique source to study the instability of the accretion disc. Our collaboration has embarked on an intensive monitoring campaign to track the spectral–temporal variability of SMC X-1 with orbital and superorbital phase resolution, during and outside superorbital excursion. This campaign – monitoring observations of SMC X-1's excursions (MOOSE) – was introduced in Dage et al. (2022).

In this paper, the second in a planned series from the MOOSE campaign, we present the detection of a new (fourth) excursion event ∼1800 d after the third excursion, and explore its connection to the spin behaviour of SMC X-1. We describe the data reduction in Section 2. The analysis results, including the time–frequency analysis of the superorbital modulation period, the spin-period variability, and the change in pulse profiles, are described in Section 3. We discuss the implications of these results in Section 4 and summarize our work in Section 5.

2 DATA PROCESSING

2.1 *Swift* BAT

The Burst Alert Telescope (BAT) onboard the *Neil Gehrels Swift Observatory* (hereafter *Swift*) has a large collecting area (5200 cm^2). The *Swift* BAT hard X-ray transient monitoring programme has recorded the X-ray count rate of known sources in the 15–50 keV band since 2004, which makes it an ideal instrument to study the superorbital modulation (Barthelmy et al. 2005; Krimm et al. 2013). We use the one-orbit light curve (with a resolution of 96 min), and eliminate data points that have uncertainties 3σ higher than the mean uncertainty. We then remove the eclipse according to the orbital ephemeris presented in Hu et al. (2019), and rebin the light curve with a 1-d resolution.

2.2 *RXTE* ASM

The All Sky Monitor (ASM) onboard the *RXTE* consists of three proportional counter arrays with a collecting area of 90 cm^2 (Levine et al. 1996). *RXTE* ended its mission in 2012, so we simply adopt data collected in Hu et al. (2019), which applied the same selection criteria as that described in Section 2.1 to investigate the superorbital modulation before MJD 55400.

2.3 MAXI GSC

The Monitor of All-sky X-ray Image (MAXI), a Japanese Experimental Module of the International Space Station, can monitor the entire sky in both X-ray (0.5–12 keV) and hard X-ray (2–30 keV) bands (Matsuoka et al. 2009). We search for pulsation using hard X-ray data collected with the Gas Slit Camera (GSC) that has a large collecting area of 5350 cm^2 and a high time resolution of 50 µs (Mihara et al. 2011). Among 12 proportional counters, we only use GSC IDs of 0, 1, 2, 4, 5, and 7 because the others are not in operation (Sugizaki et al. 2011). After 2020 August, camera 0 is also closed due to gas leakage (Mihara, Tsunemi & Negoro 2022). We extract X-ray photons in the 2–20 keV band using `mxextract` from the MAXI data base. The photon arrival times are corrected to the barycentre of the Solar system according to the ephemeris DE-200. The source photons are extracted from a 1°-radius circle centred on SMC X-1 that guarantees $\gtrsim$90 per cent of source photons are selected (Mihara et al. 2011).

3 ANALYSIS AND RESULTS

3.1 Superorbital excursion

The most recent analysis of the superorbital modulation of SMC X-1 was carried out by Dage et al. (2019) and Hu et al. (2019). Here, we extend the monitoring for an additional 4 yr until 2022 August (MJD 59810). To trace the superorbital evolution, we adopt the stacked Hilbert–Huang transform (HHT) proposed in Hu et al. (2022). The HHT, a novel and continually developed time–frequency analysis technique (Huang et al. 1998; Wu & Huang 2009), has been successfully applied to the all-sky monitoring data of SMC X-1 (see e.g. Hu et al. 2011, 2019). The HHT algorithm is sensitive to data gaps. To address this issue, we use piecewise cubic Hermite interpolation to fill in gaps in the data and assume a Gaussian uncertainty with σ equal to the mean value of other data points (Kahaner, Moler & Nash 1989). The stacked HHT, which has been used to characterize the properties of gravitational wave signals, provides a good balance between maximizing the resolution in both the time and frequency domains and eliminating possible spurious frequency modulation caused by noise and mode splitting (see Hu et al. 2022, for details).

In brief, we perform 10^4 Monte Carlo simulations. In each simulation, we create a light curve according to the observed count rates and implement white noise with standard deviations equal to the uncertainty. Then, we use the complementary ensemble empirical mode decomposition (EEMD) to decompose the light curves into a finite number of intrinsic mode functions (Yeh, Shieh & Huang 2010). This fast algorithm has been included in a MATLAB package developed by the Research Center for Adaptive Data Analysis at National Central University (Wang et al. 2014). Finally, we obtain

Downloaded from https://academic.oup.com/mnras/article/520/3/3436/7028790 by National Central University user on 24 February 2023

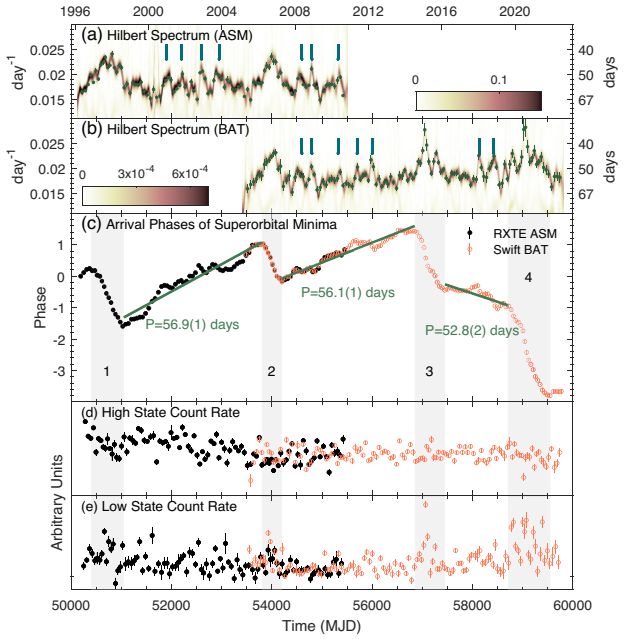

Figure 1. Stacked HHT spectra obtained with *RXTE* ASM (a) and *Swift* BAT (b), the phase evolution of the superorbital modulation (c), and corresponding high-state (d) and low-state (e) count rates of SMC X-1. Grey shaded areas in panels (c)–(e) denote the time intervals of four excursion events (numbered 1–4). Colours in Hilbert spectra denote the Hilbert amplitude. Blue vertical lines in panels (a) and (b) indicate possible mini-excursions. Green data points in panels (a) and (b) are the frequency of each superorbital cycle derived from the cycle length between two consecutive minima in panel (c). Green lines in panel (c) are best-fitting linear models of three non-excursion epochs, where corresponding periods are labelled. The slight differences in the averaged periods between epochs are much smaller than the period change between superorbital cycles, and therefore cannot be seen in the Hilbert spectra. The high- and low-state count rates are scaled to roughly the same level for display purposes.

10^4 time–frequency maps and stack them together. The resulting time–frequency maps obtained with both ASM and BAT data are shown in Fig. 1(a).

In addition, we trace the arrival times of the superorbital minima, which are obtained from the EEMD band-pass filtered light curve (see Hu et al. 2019). Assuming a folding period of 54.3 d, we performed a phase-coherent analysis on the arrival phase of the superorbital minima, which is shown in Fig. 1(c). We calculate cycle lengths between two consecutive minima and show the corresponding frequency in Fig. 1(a), suggesting that the result of the phase-coherent analysis is fully consistent with that of the HHT. From both the time–frequency map and the phase evolution, three known excursion events (first–third) are clearly seen. A new fourth excursion occurred in 2020–2021 and is found in this analysis. The starting time of each excursion, which is defined as the starting point of phase drop, is listed in Table 1. Time intervals between the onsets of the first three excursions are 3400 and 3050 d. However, the time interval between the onset of the third and fourth excursions is 1850 d, roughly half of the recurrent time-scale observed in previous events. The baseline of the superorbital period in non-excursion epochs before the fourth excursion seems to increase with time (Fig. 1). These suggest the unpredictable nature of the excursion of SMC X-1, and hint that SMC X-1 is entering a different mode of disc precession.

Finally, we calculate the count rates in the superorbital high and low states (Hu et al. 2019; Dage et al. 2022). Since the energy ranges between ASM and BAT are quite different, we scaled and shifted the light curves to compare the relative variability, as shown in Fig. 1(d). As described in Hu et al. (2019), the low-state count rate increased in the first–third excursions, but the high-state count rate remained stable. We find that the behaviour of high- and low-state count rates in the fourth excursion agrees with previous events. The lack of change in the high-state count rate suggests a stable mass accretion rate. On the other hand, the low-state count rate significantly increases during excursions, implying a possible change in the disc configuration.

3.2 Spin-period evolution

Following the algorithm in Hu et al. (2019), we employ a two-dimensional Z_2^2 test (Buccheri et al. 1983) to search for spin frequency (ν)–spin-up rate ($\dot{\nu}$) pairs within each superorbital high state and eliminate the orbital Doppler effects using MAXI GSC data. For each segment of data, we search for possible combinations of ν–$\dot{\nu}$ pairs near the predicted value based on the result of the previous superorbital high state with an oversampling factor of 10. Then, we use a finer resolution with an oversampling factor of 1000 to determine the peak location in the candidate detection. The determined ν and $\dot{\nu}$ are plotted in Figs 2(b) and (d). The uncertainties of ν and $\dot{\nu}$ are conservatively estimated from the width of the peak in the Z_2^2 spectrum.

We see a monotonically increasing trend of the spin frequency. We display the local linear trend of the spin-period evolution derived before 2019 (MJD 58484) in Fig. 2(b), and then obtain the residual in Fig. 2(c) to make a fair comparison with the evolution in Hu et al. (2019). The spin-up rate varies between neighbouring cycles in the range of 2 and 3 $\times$ 10^{-11} Hz s^{-1} through the entire MAXI observation. Interestingly, a significant spin-up rate increment, from 2.5 to 3.4 $\times$ 10^{-11} Hz s^{-1}, is seen in MJD 58400–MJD 58700, just before the onset of the fourth excursion. Then, the source takes another 200 d to decrease back. This makes the spin frequency deviate rapidly from the linear trend as shown in Fig. 2(c). This phenomenon is not observed in the third excursion but is similar to the offset between the spin-period measurements and the linear trend observed in the first excursion (İnam et al. 2010; Dage et al. 2019).

3.3 Pulse profile evolution

We investigate the long-term evolution of the 2–20 keV pulse profile using the MAXI data. We first accumulate all the photons collected in a total of 89 superorbital high states, fold them with their best local timing solution, and stack them together to obtain an averaged pulse profile (see Fig. 3a). The background level is estimated using photons collected within 1.5–2 deg from the position of SMC X-1, scaled to the same area in the sky and subtracted from the folded light curve. The pulse profile shows a typical double-peaked structure, consistent with previous works with pointed observations (see e.g. Neilsen, Hickox & Vrtilek 2004; Hickox & Vrtilek 2005; Brumback et al. 2022). The primary peak lasts for 0.55 cycles and another smaller peak lasts for 0.45 cycles. The profile can be mathematically described by two Gaussian functions (Fig. 3a).

To further trace the evolution of the pulse profile, we stack the profile every four superorbital cycles for visualization purposes and plot them in Fig. 3(b). The overall structure does not change significantly although minor variability possibly exists. Such variability cannot be directly quantified by eye. Therefore, we parametrize the pulse profiles using three quantities: the PF, the phase separation, and the ratio between two peaks, in order to follow the pulse profile evolution in more detail. We create pulse profiles from two

Downloaded from https://academic.oup.com/mnras/article/520/3/3436/7028790 by National Central University user on 24 February 2023

Table 1. Summary of superorbital excursions of SMC X-1.

Excursions	First	Second	Third	Fourth
Onset MJD	50400	53800	56850	58700
Duration (days)	650	400	600	850
Interval[a] (days)	∼1300–1700(?)	3400	3050	1850
Spin-up acceleration	Yes	...	No	Yes
Low-state count rate	Increase	Increase	Increase	Increase
High-state count rate	Stable	Stable	Stable	Stable
PF	...	...	Increase	Increase

[a]Time interval between the onset of this excursion and that of the previous excursion.

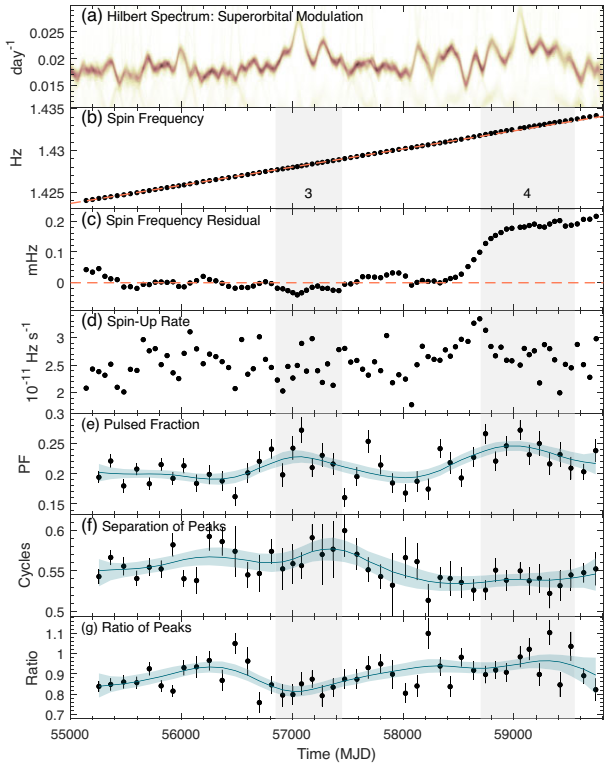

Figure 2. Evolution of the spin frequency and the pulse profile parameters of SMC X-1 obtained with MAXI. The stacked HHT spectrum obtained with *Swift* BAT is shown in panel (a) for reference. Panel (b) shows the spin period in each superorbital high state, where the orange dashed line denotes the best-fitting linear model obtained using data before MJD 5484. The residual after subtracting the linear trend and the spin-up rate are shown in panels (c) and (d), respectively. The evolution of the PF (e), phase separation of two peaks (f), and the ratio of the two peaks (g) are shown in the following panels. Grey shaded area denotes the epochs of the third and fourth excursions. Blue curves are obtained from EEMD band-pass filtered data, where the light blue areas correspond to 1σ confidence intervals.

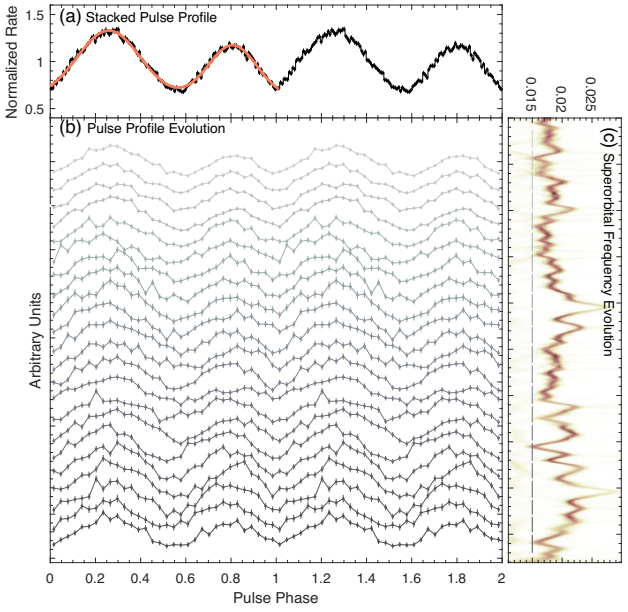

Figure 3. The 2–20 keV pulse profile evolution in the superorbital high state of SMC X-1. The stacked profile obtained from all 89 high states with MAXI is shown in panel (a). The bin size is 128 bins per cycle, and we plotted two cycles for visualization purposes. The best-fitting two-Gaussian model is plotted as the orange curve. The stacked profiles of every four consecutive superorbital high states are shown in panel (b) with 32 bins per cycle. Pulse profiles obtained from different epochs are denoted in different colours, where corresponding time intervals are shown as coloured straight lines in the stacked HHT spectrum of the superorbital modulation in panel (c).

consecutive superorbital cycles to keep enough photons in each profile. The PFs are calculated using the Fourier-based root-mean-square PF (see definition and discussion in Dib, Kaspi & Gavriil 2009; An et al. 2015). The separation and count rate ratio between the two peaks are obtained from the fitting result of two Gaussian functions. The uncertainties of all the parameters are obtained from 10^4 times Monte Carlo simulations.

The evolution of PF, peak separation, and count rate ratio are shown in Figs 2(e), (f), and (g), respectively. To further explore the evolutionary trends of parameters and eliminate short-term variability, we draw the EEMD band-pass filtered result and corresponding 1σ confidence intervals. The PF evolution is probably the most intriguing because it shows long-term variability, where the PF increases during both excursions 3 and 4. The other two parameters also show possible long-term variability although no clear connection to the superorbital or spin frequencies can be seen. We note that the pulse profile of SMC X-1 changes with both orbital and superorbital phases (see e.g. Naik & Paul 2004; Neilsen et al. 2004; Brumback et al. 2022). Therefore, these results are only valid for long-term time-averaged behaviour.

4 DISCUSSION

4.1 The fourth superorbital excursion

Within the radiation-driven warping framework, SMC X-1 is expected to show a complex disc-warp configuration, likely a

Downloaded from https://academic.oup.com/mnras/article/520/3/3436/7028790 by National Central University user on 24 February 2023

superposition of multiple warping modes and with a resultant warp shape that is time variable, possibly in an aperiodic or quasi-periodic manner (Ogilvie & Dubus 2001). A time-variable warp shape would lead to time variation in the phasing of features in the superorbital profile and a change in the instantaneous superorbital period. Both are strongly present in 1996–2021 interval analysed here (Fig. 1). Indeed, the superorbital modulation time-scale as traced by the HHT indicates a number of 'mini-excursions' (Fig. 1 panels a and b). It is the apparent ramps in the phasing of the superorbital minima, followed by rapid, monotonic evolution to earlier superorbital phases, that suggest the superorbital excursions might be different in character from the mini-excursions.

Using changes in both the superorbital phasing and the instantaneous period as tracers, our analysis of the superorbital modulation shows a new excursion in 2020–2021 with a significantly shorter waiting time, longer duration, and a possibly shorter superorbital period in the pre-excursion epochs compared to previous excursions. Under the warped-disc model, the superorbital modulation is caused by the variation in the absorption column and/or covering fraction of the central X-ray emission region. Then, a change in the warp configuration would result in a change in the low-state flux, which has now been seen in all four superorbital excursions analysed. Analysis of recent soft X-ray observations taken at a variety of superorbital phases as part of our programme also shows corroborating evidence for this model (Karam et al., in preparation). We note also that Pradhan, Maitra & Paul (2020) find evidence from superorbital phase-resolved joint Suzaku/*NuSTAR* spectroscopic fits that indeed superorbital variation in partial covering fraction of the inner disc regions is a more likely mechanism than varying absorption column density. However, they go on to argue that the varying instantaneous accretion rate is a more likely mechanism for the superorbital modulation than any kind of varying obscuration. If indeed it is instantaneous $\dot{M}$ on to the accretor that varies with superorbital phase, then the lack of significant superorbital variation in the spin period (as opposed to the pulse profile) seen in Pradhan et al. (2020) is puzzling.

Dedicated soft X-ray observations in the superorbital low state during and out-of-excursion epochs may be required to verify the change of the soft X-ray component, which would be contributed by the reprocessed X-rays from the inner accretion disc, in the low states during and out of excursions (Hickox, Narayan & Kallman 2004).

The most intriguing feature of the fourth excursion is the acceleration of the spin-up rate, which is not seen in the third excursion but observed in the first excursion. A change in the accretion torque is expected to accompany a change in the warp inclination. The 1-yr time delay between the onset of the spin-up acceleration and the fourth superorbital excursion implies a possible inside-out process between the change in accretion torque and the warp inclination. A similar time delay is possibly seen in the first excursion (Dage et al. 2019).

4.2 Variation in pulse profile

The SMC X-1 pulse profile is thought to trace different components in the system. The *hard* pulse profile likely arises from a direct line-of-sight view of the accretor itself, while the *soft* pulsed component may come from reprocessing of hard X-ray emission by the inner disc (Hickox et al. 2004; Neilsen et al. 2004; Brumback et al. 2022, and references therein). In a single 2–20 keV energy range, we do not have sensitivity to the hard and soft X-ray pulse profiles separately. All of the pulse profiles we report here were taken in the superorbital high state, corresponding to the most direct view of the accretor and maximum opening angle of the inner disc. Thus, our experiment presents 89 samples of the 2–20 keV pulse profile with the inner disc in roughly the same orientation in three dimensions with respect to the line of sight.

Our pulse profile data provide coverage for the third and fourth excursions. There is evidence that the PF increases for both superorbital excursions, which is generally consistent with a model in which the inner disc configuration indeed changes during the superorbital excursion (Fig. 2, panel e), or perhaps that the stream impact point(s) on the neutron star changes with superorbital cycle length.

There is some room for improvement in the pulse profile analysis. For example, the timing solution is a simple first-order spin-up model within a few tens of days. A time-variable timing noise between superorbital cycles would distort the observed pulse profile under such an oversimplified timing solution. Future observations that can derive a (semicoherent) phase-connected timing solution on a shorter time-scale would help clarify the evolution of the pulse profile.

4.3 Accretion and disc variation

Taken as a set, the four superorbital excursions do not suggest a simple, causative link between disc warp behaviour and accretion rate on to the neutron star that is suggested by the warped-disc model (Wijers & Pringle 1999; Still & Boyd 2004). While the first and fourth superorbital excursions are preceded by spin-up acceleration, the third excursion does not show any pre-excursion spin-up trend: indeed, for the third excursion the superorbital and spin modulations appear completely uncoupled (the second excursion does not have sufficient spin-period coverage to make any inferences). This suggests that either the apparent pre-excursion spin-up increase of the neutron star in the first and fourth excursions is merely a coincidence or there might be a threshold below which the two behaviours are not strongly coupled. The mechanism for such a threshold is not at present clear: from the limited sample of superorbital excursions, we note that the first and fourth excursions that show spin-up acceleration have a duration longer than the other two events. These may hint at various triggering mechanisms of the superorbital excursion. Another feature commonly seen in both the first and fourth excursions is the waiting time interval. The Burst And Transient Source Experiment observation revealed a possible excursion event that ended at MJD 49100 (zeroth excursion) though the complete excursion was not clearly observed (see fig. 2 in Clarkson et al. 2003a). If this is true and the duration of the zeroth excursion has a similar time-scale of 400–800 d, the time interval between the zeroth and first excursions would be roughly 1300–1700 d, similar to the time interval between the third and fourth excursions. We also note that a mini-excursion may occur before the fourth excursion, and the onset of the spin-up acceleration coincides with the end of this mini-excursion. Such mini-excursions are probably seen in 2004, 2008, and 2012, but no corresponding change in the spin-up rate was observed in the 2012 event (see Figs 1 and 2). Monitoring the spin-up rate and the superorbital period with all-sky monitoring programs would increase samples of superorbital excursions and help test their connection.

Finally, it was suggested that behaviour of SMC X-1's warp may be similar to that of Her X-1, which shows a connection between its pulse profile and superorbital modulation amplitude (Still & Boyd 2004). Her X-1's superorbital profile is double peaked, with flux at the brighter peak correlated to the superorbital period (Leahy & Igna 2010). Moreover, its spin frequency occasionally decreases, particularly during anomalous low states (Staubert et al. 2009, 2013). These suggest that Her X-1's warp angle can sometimes be extremely high ($>90^\circ$), resulting in a negative accretion torque (Parmar et al.

Downloaded from https://academic.oup.com/mnras/article/520/3/3436/7028790 by National Central University user on 24 February 2023

1999). Monitoring Her X-1's spin frequency change within one superorbital cycle reveals a sub-microsecond change with a 35-d period, suggesting a free precession of the axis of the neutron star (Kolesnikov, Shakura & Postnov 2022). However, these behaviours are not observed in SMC X-1. The high-state flux remained stable during all excursions, implying a stable mass accretion rate. In addition, the increase in the low-state flux suggests a possible change in the warp or partial covering fraction, inferring a possible change in the spin frequency. Although both SMC X-1 and Her X-1 show variations in their soft pulse profile shape consistent with precession of a warped accretion disc (Brumback et al. 2020, 2021), the binaries fundamentally differ in their mass transfer mechanisms. Her X-1's smaller A/F stellar companion transfers gas to the neutron star via Roche lobe overflow, whereas SMC X-1's B0 supergiant star likely also has stellar winds that complicate the mass transfer process (Webster et al. 1972; Reynolds et al. 1997). Therefore, the superorbital modulation of SMC X-1 could be a combination of obscuring by warped accretion disc and other effects such as the change in partial covering fraction of the inner disc (Pradhan et al. 2020; Brumback et al. 2022). Other models, such as the precession of ring tube, the precession of funnel-shaped wind, or change in mass accretion rate, can possibly explain the superorbital modulation in SMC X-1 (Tsygankov et al. 2016; Dauser et al. 2017; Inoue 2019). Future theoretical works are needed to test whether the observed phenomena, especially the connection between the spin and the superorbital modulations, can be observed in the model.

5 SUMMARY

We perform a detailed analysis of the evolution of SMC X-1's superorbital modulation period and extend the time baseline to 26 yr. We find a fourth superorbital excursion, which has the longest duration and the shortest waiting time among all confirmed events. Moreover, we find a clear spin-up acceleration before the onset of the fourth excursion, implying a possible inside-out process. This phenomenon is only seen in the first and fourth excursions but not in the third event, suggesting possible different triggering mechanisms or some threshold that reveals the spin–superorbital connection. Monitoring the spin and superorbital behaviours of SMC X-1 and detailed timing and spectral observations in the following years are essential to reveal the underlying physics of the accretion in this system and provide links to other systems such as PULXs. We encourage further theoretical studies to understand the conditions for producing observed connections between spin and superorbital modulations and observations to test whether these behaviours can be seen in other systems.

ACKNOWLEDGEMENTS

We thank the anonymous reviewer for valuable comments that improved this paper. This work made use of data provided by the ASM/*RXTE* teams at MIT and the *RXTE* Science Operations Facility (SOF) and Guest Observer Facility (GOF) at Goddard Space Flight Center (GSFC) of the National Aeronautics and Space Administration (NASA), the *Swift* BAT data provided by the Hard X-ray Transient Monitor (Krimm et al. 2013), and the MAXI data provided by RIKEN, Japan Aerospace Exploration Agency (JAXA), and the MAXI team. CPH acknowledges support from the National Science and Technology Council in Taiwan through grant MOST 109-2112-M-018-009-MY3. KCD acknowledges fellowship funding from Fonds de Recherche du Québec-Nature et Technologies, Bourses de recherche postdoctorale B3X no. 319864. DH acknowledges funding from the Natural Sciences and Engineering Research Council of Canada (NSERC) and the Canada Research Chairs (CRC) program.

DATA AVAILABILITY

The *RXTE* ASM light curve can be downloaded from the ASM Source Catalog (https://heasarc.gsfc.nasa.gov/docs/xte/ASM/sources.html). The *Swift* BAT light curve (Krimm et al. 2013) is publicly available from the *Swift*/BAT Hard X-ray Transient Monitor programme web page (https://swift.gsfc.nasa.gov/results/transients/). The MAXI GSC data can be downloaded and processed using the MAXI software package, which has been implemented within HEASOFT (https://heasarc.gsfc.nasa.gov/docs/software/heasoft/) since version 6.25. The spin frequency measurements of this work are archived on this web page maintained by the MAXI team at RIKEN (http://maxi.riken.jp/pulsar/smcx1/).

REFERENCES

An H. et al., 2015, ApJ, 807, 93
Bachetti M. et al., 2014, Nature, 514, 202
Barthelmy S. D. et al., 2005, Space Sci. Rev., 120, 143
Brightman M. et al., 2020, ApJ, 895, 127
Brumback M. C., Hickox R. C., Fürst F. S., Pottschmidt K., Tomsick J. A., Wilms J., 2020, ApJ, 888, 125
Brumback M. C., Hickox R. C., Fürst F. S., Pottschmidt K., Tomsick J. A., Wilms J., Staubert R., Vrtilek S., 2021, ApJ, 909, 186
Brumback M. C. et al., 2022, ApJ, 926, 187
Buccheri R. et al., 1983, A&A, 128, 245
Charles P., Clarkson W., Cornelisse R., Shih C., 2008, New Astron. Rev., 51, 768
Clarkson W. I., Charles P. A., Coe M. J., Laycock S., Tout M. D., Wilson C. A., 2003a, MNRAS, 339, 447
Clarkson W. I., Charles P. A., Coe M. J., Laycock S., 2003b, MNRAS, 343, 1213
Dage K. C., Clarkson W. I., Charles P. A., Laycock S. G. T., Shih I.-C., 2019, MNRAS, 482, 337
Dage K. C. et al., 2022, MNRAS, 514, 5457
Dauser T., Middleton M., Wilms J., 2017, MNRAS, 466, 2236
Dib R., Kaspi V. M., Gavriil F. P., 2009, ApJ, 702, 614
Falanga M., Bozzo E., Lutovinov A., Bonnet-Bidaud J. M., Fetisova Y., Puls J., 2015, A&A, 577, A130
Foulkes S. B., Haswell C. A., Murray J. R., 2010, MNRAS, 401, 1275
Gruber D. E., Rothschild R. E., 1984, ApJ, 283, 546
Hickox R. C., Vrtilek S. D., 2005, ApJ, 633, 1064
Hickox R. C., Narayan R., Kallman T. R., 2004, ApJ, 614, 881
Hu C.-P., Chou Y., Wu M.-C., Yang T.-C., Su Y.-H., 2011, ApJ, 740, 67
Hu C.-P., Li K. L., Kong A. K. H., Ng C.-Y., Chun-Che Lin L., 2017, ApJ, 835, L9
Hu C.-P., Mihara T., Sugizaki M., Ueda Y., Enoto T., 2019, ApJ, 885, 123
Hu C.-P., Lin L. C.-C., Pan K.-C., Li K.-L., Yen C.-C., Kong A. K. H., Hui C. Y., 2022, ApJ, 935, 127
Huang N. E. et al., 1998, R. S. London Proc. Ser. A, 454, 903
İnam S. c., Baykal A., Beklen E., 2010, MNRAS, 403, 378
Inoue H., 2019, PASJ, 71, 36
Kahaner D., Moler C., Nash S., 1989, Numerical Methods and Software. Prentice Hall, Englewood Cliffs, NJ
King A., Lasota J.-P., 2019, MNRAS, 485, 3588
Kolesnikov D., Shakura N., Postnov K., 2022, MNRAS, 513, 3359
Kong A. K. H., Hu C.-P., Lin L. C.-C., Li K. L., Jin R., Liu C. Y., Yen D. C.-C., 2016, MNRAS, 461, 4395
Krimm H. A. et al., 2013, ApJS, 209, 14
Leahy D. A., Igna C. D., 2010, ApJ, 713, 318
Levine A. M., Bradt H., Cui W., Jernigan J. G., Morgan E. H., Remillard R., Shirey R. E., Smith D. A., 1996, ApJ, 469, L33
Lucke R., Yentis D., Friedman H., Fritz G., Shulman S., 1976, ApJ, 206, L25

Downloaded from https://academic.oup.com/mnras/article/520/3/3436/7028790 by National Central University user on 24 February 2023

Matsuoka M. et al., 2009, PASJ, 61, 999
Mihara T. et al., 2011, PASJ, 63, S623
Mihara T., Tsunemi H., Negoro H., 2022, MAXI : Monitor of All-sky X-ray Image, in C. Bambi A. Santangeloeds, Handbook of X-ray and Gamma-ray Astrophysics, Springer, Singapore, ISBN: 9789811969591
Naik S., Paul B., 2004, A&A, 418, 655
Neilsen J., Hickox R. C., Vrtilek S. D., 2004, ApJ, 616, L135
Ogilvie G. I., Dubus G., 2001, MNRAS, 320, 485
Parmar A. N., Oosterbroek T., dal Fiume D., Orlandini M., Santangelo A., Segreto A., del Sordo S., 1999, A&A, 350, L5
Pike S. N. et al., 2019, ApJ, 875, 144
Pradhan P., Maitra C., Paul B., 2020, ApJ, 895, 10
Pringle J. E., 1996, MNRAS, 281, 357
Reynolds A. P., Hilditch R. W., Bell S. A., Hill G., 1993, MNRAS, 261, 337
Reynolds A. P., Quaintrell H., Still M. D., Roche P., Chakrabarty D., Levine S. E., 1997, MNRAS, 288, 43
Staubert R., Klochkov D., Postnov K., Shakura N., Wilms J., Rothschild R. E., 2009, A&A, 494, 1025
Staubert R., Klochkov D., Vasco D., Postnov K., Shakura N., Wilms J., Rothschild R. E., 2013, A&A, 550, A110
Still M., Boyd P., 2004, ApJ, 606, L135
Sugizaki M. et al., 2011, PASJ, 63, S635
Thomas J. K., Charles P. A., Buckley D. A. H., Kotze M. M., Lasota J.-P., Potter S. B., Steiner J. F., Paice J. A., 2022, MNRAS, 509, 1062
Trowbridge S., Nowak M. A., Wilms J., 2007, ApJ, 670, 624
Tsygankov S. S., Mushtukov A. A., Suleimanov V. F., Poutanen J., 2016, MNRAS, 457, 1101
Vasilopoulos G., Koliopanos F., Haberl F., Treiber H., Brightman M., Earnshaw H. P., Gúrpide A., 2021, ApJ, 909, 50
Walton D. J. et al., 2016, ApJ, 827, L13
Wang Y.-H., Yeh C.-H., Young H.-W. V., Hu K., Lo M.-T., 2014, Phys. A Stat. Mech. Appl., 400, 159
Webster B. L., Martin W. L., Feast M. W., Andrews P. J., 1972, Nat. Phys. Sci., 240, 183
Wijers R. A. M. J., Pringle J. E., 1999, MNRAS, 308, 207
Wojdowski P., Clark G. W., Levine A. M., Woo J. W., Zhang S. N., 1998, ApJ, 502, 253
Wu Z., Huang N. E., 2009, Adv. Adapt. Data Anal., 1, 1
Yeh J.-R., Shieh J.-S., Huang N. E., 2010, Adv. Adapt. Data Anal., 02, 135
van der Meer A., Kaper L., van Kerkwijk M. H., Heemskerk M. H. M., van den Heuvel E. P. J., 2007, A&A, 473, 523

This paper has been typeset from a TEX/LATEX file prepared by the author.

Downloaded from https://academic.oup.com/mnras/article/520/3/3436/7028790 by National Central University user on 24 February 2023